

Fusion reaction studies for the ${}^9\text{Be} + {}^{89}\text{Y}$ system at above-barrier energies

G. S. Li¹, M. L. Liu,^{1,*} D. Patel,^{1,†} Y. D. Fang,¹ X. H. Zhou,¹ Y. H. Zhang,¹ A. Diaz-Torres,² C. S. Palshetkar,³ J. Lubian,⁴ N. T. Zhang,¹ J. G. Wang,¹ B. S. Gao,¹ Y. H. Qiang,¹ S. Guo,¹ Y. Zheng,¹ K. L. Wang,¹ K. K. Zheng,¹ R. Li,¹ and S. Mukherjee⁵

¹*Institute of Modern Physics, Chinese Academy of Sciences, Lanzhou 730000, People's Republic of China*

²*Department of Physics, University of Surrey, Guildford GU2 7XH, United Kingdom*

³*Department of Nuclear and Atomic Physics, Tata Institute of Fundamental Research, Mumbai 400005, India*

⁴*Instituto de Física, Universidade Federal Fluminense, Avenida Litorânea s/n, Gragoatá, Niterói, Rio de Janeiro 24210-340, Brazil*

⁵*Physics Department, Faculty of Science, M. S. University of Baroda, Vadodara 390002, India*



(Received 3 June 2019; revised manuscript received 31 October 2019; published 10 January 2020)

Complete fusion (CF) cross section measurement for the weakly bound ${}^9\text{Be}$ projectile interacting with the intermediate mass target ${}^{89}\text{Y}$ has been extended to energies greater than the fusion barrier, by implementing off-line characteristic γ -ray detection techniques. The available experimental data for the ${}^9\text{Be} + {}^{89}\text{Y}$ reaction system were compared with the theoretical predictions, using the PLATYPUS code that is based on a classical dynamical model. By introducing the breakup probability that deduced in the literature from the fitting of the experimental data, the model managed to reproduce the CF cross sections of ${}^9\text{Be}$ beam with targets of different atomic mass. Through the study, it is revealed that the extended CF excitation function for the ${}^9\text{Be} + {}^{89}\text{Y}$ system is consistent with the systematical behavior that the prompt-breakup probability at above-barrier energies is roughly independent of the target in the reactions induced by the same weakly bound projectiles.

DOI: [10.1103/PhysRevC.101.014606](https://doi.org/10.1103/PhysRevC.101.014606)

I. INTRODUCTION

Investigations on the breakup and/or transfer coupling effects of weakly bound projectile nuclei such as ${}^6,7\text{Li}$, ${}^9\text{Be}$ have been a topic of great interest for the understanding of astrophysical processes and the production of nuclei near the drip line [1–3]. Due to the low beam intensity and poor statistics of radioactive ion beams, the stable weakly bound nuclei with high intensity are usually chosen for studying the unusual features such as large breakup probabilities and their effects on different reaction channels, mainly fusion and elastic. The mechanism of fusion reaction that involves weakly bound nuclei is actually associated with several processes. For example, the complete fusion (CF) of the projectile with the target, the incomplete fusion (ICF) where one or more fragments of the projectile are captured by the target, and the sequential fusion (SCF) where all the fragments after the breakup are fused with the target. The sum of ICF + SCF + CF is called total fusion (TF). However, it is important to note that the SCF and the CF processes cannot be distinguished in the experiment and thus experimentally CF is the sum of these two processes.

By measuring the fusion cross sections one can study its enhancement or suppression owing to breakup and/or transfer coupling effects at the energies around the Coulomb barrier. A detailed literature study revealed that the TF cross sections

are not suppressed at the above-the-Coulomb barrier energies as it actually includes ICF, which is a part of the flux due to the breakup and/or transfer reactions. On the contrary, the coupling effects of breakup and/or transfer channels on the complete fusion (CF) suppress its cross section at energies above the Coulomb barrier and produce some enhancements at sub-barrier energies in comparison to the coupled channels calculations that do not take into account coupling effects [4–8]. Many efforts have been devoted to investigate the systematic of the CF features [9–15]. In these studies, one conclusion is that the suppression factor of the CF cross section at energies above the Coulomb barrier is independent of the mass of the target, and depends mainly on the projectile breakup threshold [9,10]. However, later studies revealed that the breakup mechanism is different in interactions with nuclei in different mass regions [11], and dedicated measurements by Cook *et al.* [12] showed a mild target dependence of the breakup probabilities. Apparently, for the CF suppression the underlying mechanism is complicated and controversial. It is also reported to be affected by other processes such as transfer-triggered breakup [16–18] and cluster transfer [19].

In the case of ${}^9\text{Be}$ projectile, most of the CF measurements are carried out with heavy mass targets such as ${}^{124}\text{Sn}$, ${}^{181}\text{Ta}$, ${}^{209}\text{Bi}$ [20–22]. For light mass targets, there is coexistence of different evaporation residues, which makes it difficult to separate CF and ICF events. For the intermediate mass targets, the ${}^9\text{Be} + {}^{89}\text{Y}$ system has been measured at near barrier [23] and above-barrier energies [24], but the suppression of CF cross section was only studied at near barrier range in Ref. [23]. In this work, we provide a new experimental result of CF for

*liuml@impcas.ac.cn

†kherdipika2006@gmail.com

the ${}^9\text{Be} + {}^{89}\text{Y}$ system up to more than two times Coulomb barrier energy and combine the previous experimental data to compare with the theoretical calculations. The present work also aims at examining the systematical behavior of the ${}^9\text{Be}$ prompt-breakup probabilities at above-the-barrier energies based on a breakup-capture picture within the PLATYPUS model [25].

The paper has been organized as follows. The experimental details and the estimation of reaction cross sections for the ${}^9\text{Be} + {}^{89}\text{Y}$ system are described in Sec. II. Section III presents the comparison of CF data with theoretical calculations. A summary of the present study is given in Sec. IV.

II. EXPERIMENTAL DETAILS AND DATA REDUCTION

The yields of the fusion evaporation products were measured by using the stacked foil activation technique, at Heavy Ion Research Facility in Lanzhou (HIRFL), China. Collimated ${}^9\text{Be}$ beam was incident on five ${}^{89}\text{Y}$ targets, having thickness ≈ 1 mg/cm², for about 12 h. The beam current was in average of 13 nA. The targets were prepared by the high-vacuum evaporation technique on Au backing of ≈ 1 mg/cm² thickness. The backing served as the catcher to trap the recoiling residues produced during the activation. The five targets/backings were put in a stack such that the one in front serves as the energy degrader of the one after, and there is no additional energy degrader between the targets/backings. Detailed descriptions of the experimental technique and setup have been presented in Ref. [26]. The initial energy, delivered by the accelerator, was 50.4 MeV. The mean beam energy incident at half the thickness on each ${}^{89}\text{Y}$ target, obtained using ATIMA calculation within the LISE++ program [27,28], was used to evaluate the cross section. Finally, the irradiation of the targets was done in energy range of 45.9–50.1 MeV, in steps of 1–1.1 MeV. A high-precision current integrator was employed to measure the beam flux deposited at the Faraday cup, placed after the target. In order to repel the secondary electrons, the Faraday cup was biased with a negative 400 V electrode on the collector. Additionally, two silicon surface-barrier detectors, mounted at $\pm 30^\circ$ to the beam direction, were used to monitor the elastic scattering of the ${}^9\text{Be}$ projectiles by a thin Au foil placed upstream from the target stack. In both cases, the profiles of the beam flux were recorded by the online data acquisition system, which can easily extract the beam intensity in intervals of 1 s. The two sets of deduced current values are in agreement with each other.

The off-line γ activity of the targets was measured using five HPGe detector groups consisting of ten HPGe detectors. In each group, the two detectors were positioned at 180° to each other. The data acquisition system was set such that single γ -ray and γ - γ coincidence measurements could be performed at the same time. The Ge crystal part of each detector was surrounded by a Pb annular cylinder of 3 cm thickness to reduce background from natural radioactivity. The same setup was used in our previous paper [29]. The energy calibration and absolute efficiency of the detectors were determined by using a set of activity calibrated radioactive sources (${}^{60}\text{Co}$, ${}^{133}\text{Ba}$, and ${}^{152}\text{Eu}$) placed at the same geometry as the targets. The activity measurements of the targets were carried out

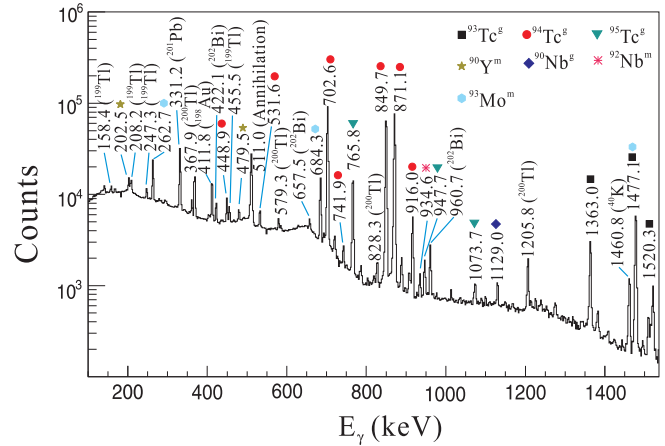


FIG. 1. Off-line γ -ray spectrum for ${}^9\text{Be} + {}^{89}\text{Y}$ system with beam energy of 50.1 MeV measured at 10.5 h after the end of the activation with a measuring time of 1 h. The γ -ray contamination, mainly from the reaction products of ${}^9\text{Be}$ with ${}^{197}\text{Au}$ target backing, are also indicated.

shortly after the activation for the short lifetime residues, and more than one month later for the long lifetime residues.

The residues for the ${}^9\text{Be} + {}^{89}\text{Y}$ reaction system observed in the present experiment are mainly from the $3n$, $4n$, and $5n$

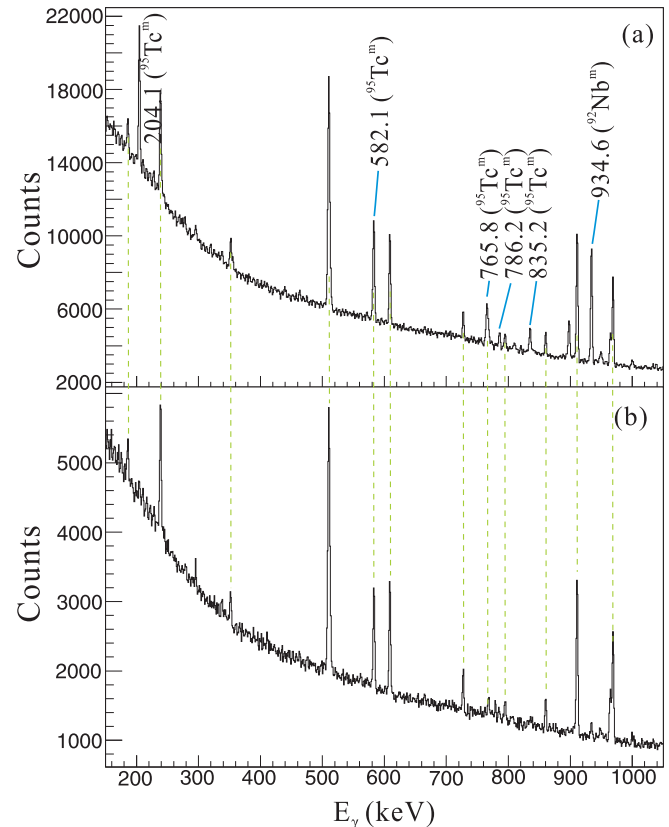


FIG. 2. (a) Off-line γ -ray spectrum for ${}^9\text{Be} + {}^{89}\text{Y}$ system with beam energy of 45.9 MeV measured at 40 days after the end of the activation with measuring a time of 69 h. (b) Background spectrum for comparison.

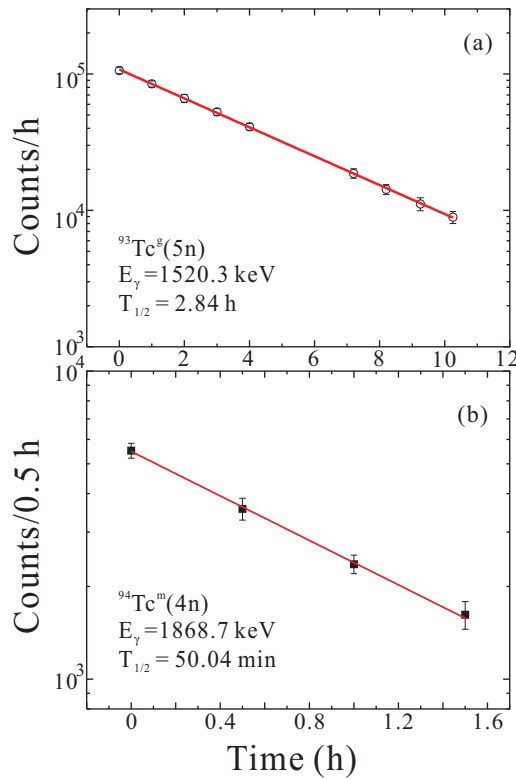


FIG. 3. Radioactive decay curves for the (a) ${}^{93}\text{Tc}^g$ and (b) ${}^{94}\text{Tc}^m$ nuclei formed in the ${}^9\text{Be} + {}^{89}\text{Y}$ reaction by using the 1520.3- and 1868.7-keV γ rays, respectively.

evaporation channels. Besides that we have also observed the $\alpha 2n$, $\alpha 4n$ as well as the $4np$ products. The residues of $\alpha 2n$ and $\alpha 4n$ may arise from CF and/or ICF processes. In the case of CF, they refer to the fusion of ${}^9\text{Be}$ with target followed by evaporation of $2n$ and $4n$ in addition to one α particle, and in the case of ICF they refer to the fusion of α fragment with the target and then evaporate $1n$ and $3n$, respectively. These nuclei were identified and crosschecked by the information of characteristic γ -ray energies, half-lives, and branching ratios, etc. Figure 1 shows the typical γ lines from short lifetime residues measured at 10.5 h after the activation. The spectra measured at 40 d after the activation are shown in Fig. 2. During the cooling period, activities of the short lifetime residues decreased significantly, and the characteristic γ lines from the long lifetime residues became visible as shown in Fig. 2(a). These γ rays could be clearly distinguished when comparing with the background spectrum shown in Fig. 2(b). For instance, the 582.1- and 765.8-keV γ rays from ${}^{95}\text{Tc}^m$ could be identified from the relative intensities, even there are peaks at corresponding positions of the background spectrum. Note that in the previous decay study of ${}^{95}\text{Tc}$ [31] the 765.8-keV γ ray was only identified in the decay of ${}^{95}\text{Tc}^g$ but not in the case of ${}^{95}\text{Tc}^m$. To confirm that the γ rays observed are coming from the interested residues, the half-life for each residues has been followed if available. As examples, the radioactive decay curves obtained for ${}^{93}\text{Tc}^g$ (1520.3 keV line) and ${}^{94}\text{Tc}^m$ (1868.7 keV line) are shown in Fig. 3(a) and 3(b), respectively. The extracted half-lives in this work are

TABLE I. List of evaporation residues identified in the present measurement along with their half-lives $T_{1/2}$, J^π , E_γ , and absolute intensities I_γ [30]. The intense γ rays (in bold) were chosen to evaluate the cross sections. The other γ rays corresponding to the same nuclei were also used to crosscheck the deduced cross-section values.

Residue	$T_{1/2}$	J^π	E_γ (keV)	I_γ (%)
${}^{93}\text{Tc}^g(5n)$	2.75 h	$9/2^+$	1363.0	66.2
			1477.1	8.7
			1520.3	24.4
			702.6	99.6
			741.9	1.21
${}^{94}\text{Tc}^g(4n)$	4.88 h	7^+	448.9	3.3
			531.6	2.35
			702.6	99.6
			741.9	1.21
			849.7	95.7
${}^{94}\text{Tc}^m(4n)$	52 min	2^+	871.1	99.9
			871.1	99.9
			916.0	7.6
			1868.7	5.7
			947.7	1.95
${}^{95}\text{Tc}^g(3n)$	20 h	$9/2^+$	765.8	93.8
			947.7	1.95
			1073.7	3.74
			204.1	63.2
			582.1	30.0
${}^{95}\text{Tc}^m(3n)$	61 d	$1/2^-$	765.8	
			786.2	8.66
			835.2	26.6
			934.6	99.2
			902.7	92.7
${}^{92}\text{Nb}^m(\alpha 2n)$	10.15 d	2^+	934.6	99.2
${}^{90}\text{Nb}^g(\alpha 4n)$	14.60 h	8^+	1129.0	92.7
${}^{93}\text{Mo}^m(4np)$	6.85 h	$21/2^+$	262.7	57.4
			684.3	99.9
			1477.1	99.1

inconsistent with the values in the literature [23,24]. Table I lists the identified residues for the ${}^9\text{Be} + {}^{89}\text{Y}$ system, along with the corresponding information of evaporation channels, half-lives, γ -ray energies, and branching ratios, etc. [30].

The experimental cross sections of products formed in the ${}^9\text{Be} + {}^{89}\text{Y}$ reaction were extracted using the half-lives, prominent γ -ray energies of decay, and intensities following the method described in Ref. [21]. The other γ rays corresponding to the same products were also used to crosscheck the accepted cross-section values. The results are given in Table II. The errors shown in the table were estimated by taking into account errors of beam intensity ($\approx 3\%$), target thickness ($\approx 3\%$), and detector efficiency ($\approx 3\%$).

III. COMPARISON OF DATA WITH THEORETICAL PREDICTIONS AND DISCUSSION

The experimental cross sections for the neutron evaporation channels following CF of ${}^9\text{Be} + {}^{89}\text{Y}$ reaction in the 19.4–50.1 MeV energy range have been compared with statistical model predictions performed using the code PACE [32] in Fig. 4. The experimental data of beam energy of 46.4 MeV and those smaller than 45.9 MeV were taken from Refs. [23,24]. The l distribution obtained from the CCFULL

TABLE II. Measured cross sections for the residues formed through the $^9\text{Be} + ^{89}\text{Y}$ reaction.

E_{lab} (MeV)	$^{93}\text{Tc}^g$ (mb)	^{94}Tc (mb)	^{95}Tc (mb)	$^{92}\text{Nb}^m$ (mb)	$^{90}\text{Nb}^g$ (mb)
50.1	109.23 ± 11.90	481.05 ± 35.49	114.77 ± 18.27	8.54 ± 0.54	2.70 ± 0.35
49.1	76.47 ± 4.22	476.13 ± 33.03	116.13 ± 14.29	12.56 ± 0.99	2.24 ± 0.30
48.1	50.82 ± 4.90	441.32 ± 26.54	120.60 ± 7.98	14.04 ± 1.11	0.83 ± 0.12
47.0	34.47 ± 2.89	436.44 ± 24.51	132.64 ± 9.74	18.59 ± 1.19	0.39 ± 0.08
45.9	27.28 ± 3.14	449.85 ± 27.47	175.81 ± 16.13	21.12 ± 1.63	

[33] calculations was fed as an input at each energy to obtain the cross sections.

In the calculation one important parameter is the level density a , calculated from the expression $a = A/K \text{ MeV}^{-1}$,

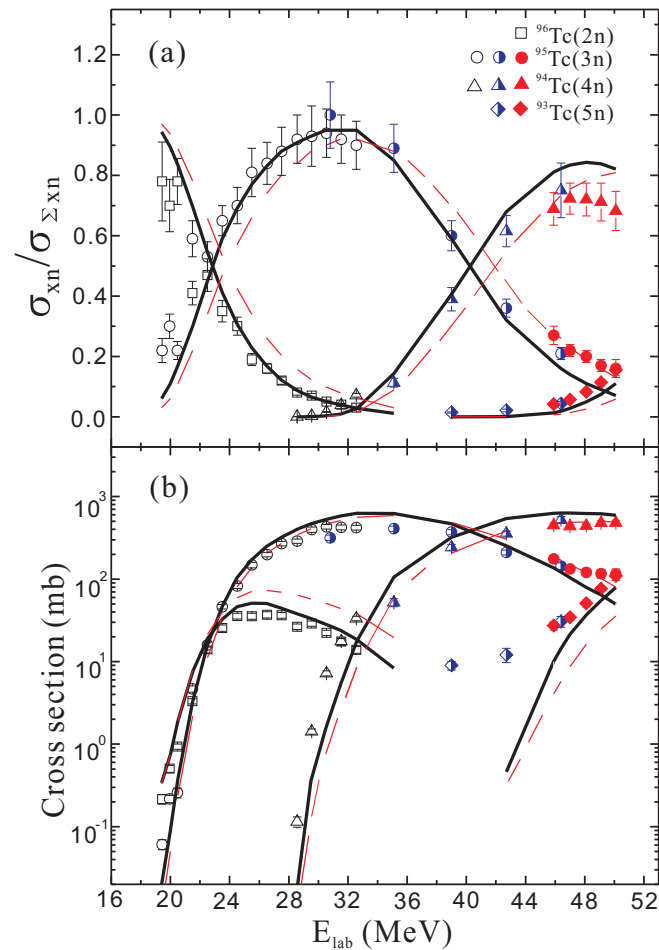


FIG. 4. (a) Experimental and PACE predicted ratios of a given complete fusion xn residue to the sum of all such residues formed through the $^9\text{Be} + ^{89}\text{Y}$ system, as a function of the beam energy. (b) Direct comparison of experimental residue cross sections with the PACE predictions. The experimental data of black hollow symbols, blue half-filled symbols, and red full-filled symbols were taken from Ref. [23], Ref. [24], and this work, respectively. Some error bars are the same size or smaller than the symbols used to represent the experimental points. The results of the theoretical calculations for the corresponding residues are shown by the black solid line and red dashed line, calculated with density parameters of $a = A/9.6 \text{ MeV}^{-1}$ and $a = A/13 \text{ MeV}^{-1}$, respectively. See text for details.

where A is the nucleon number of the compound system and K is free parameter. The ratios of $\sigma_{xn}/\sigma_{\Sigma xn}$ ($x = 2, 3, 4, 5$) were calculated using two different values of $K = 9.6$ and 13 , and compared with the corresponding experimental data in Fig. 4(a). One can see that the parameter of $K = 9.6$, adopted in the previous work [23], can nicely reproduce the ratio of σ_{3n}/σ_{2n} but has to be bigger in order to well predict the σ_{4n}/σ_{3n} ratios in the extended energy region of present measurement. All the available experimental cross sections were also compared directly with the PACE predictions in Fig. 4(b). One can see that, using the parameter of $K = 9.6$, the peaks of $2n$, $3n$, and $4n$ evaporation channels were all overestimated at their peaks, even the σ_{3n}/σ_{2n} ratios were well predicted. This is possibly caused by the overestimation of the total cross sections by the PACE code. For the $5n$ channel residue of ^{93}Tc ,

TABLE III. Measured cross section of complete fusion along with the ratio R (see text for definition) obtained from PACE for the $^9\text{Be} + ^{89}\text{Y}$ system.

E_{lab} (MeV)	R	$\sigma_{\text{fus}}^{\text{expt}}$ (mb)
50.1 ^a	0.62	1142 ± 67
49.1 ^a	0.63	1063 ± 58
48.1 ^a	0.64	952 ± 44
47.0 ^a	0.66	912 ± 40
46.4 ^b	0.67	1045 ± 77
45.9 ^a	0.68	966 ± 47
42.7 ^b	0.72	804 ± 40
39.0 ^b	0.77	813 ± 44
35.1 ^b	0.81	566 ± 36
32.6 ^c	0.84	559 ± 32
31.5 ^c	0.85	541 ± 33
30.5 ^c	0.85	538 ± 32
29.5 ^c	0.87	494 ± 35
28.6 ^c	0.87	361 ± 20
27.5 ^c	0.88	347 ± 20
26.5 ^c	0.89	265 ± 14
25.5 ^c	0.89	206 ± 13
24.5 ^c	0.90	132 ± 7
23.5 ^c	0.90	80 ± 4
22.5 ^c	0.90	33 ± 2
21.5 ^c	0.91	8.8 ± 0.5
20.5 ^c	0.91	1.3 ± 0.1
20.0 ^c	0.90	0.8 ± 0.06
19.4 ^c	0.92	0.3 ± 0.03

^aThis work.

^bThe data of $\sigma_{2n+3n+4n+5n}^{\text{expt}}$, used to deduce the cross section of complete fusion, is taken from Ref. [24].

^cThe data of $\sigma_{2n+3n+4n+5n}^{\text{expt}}$ is taken from Ref. [23].

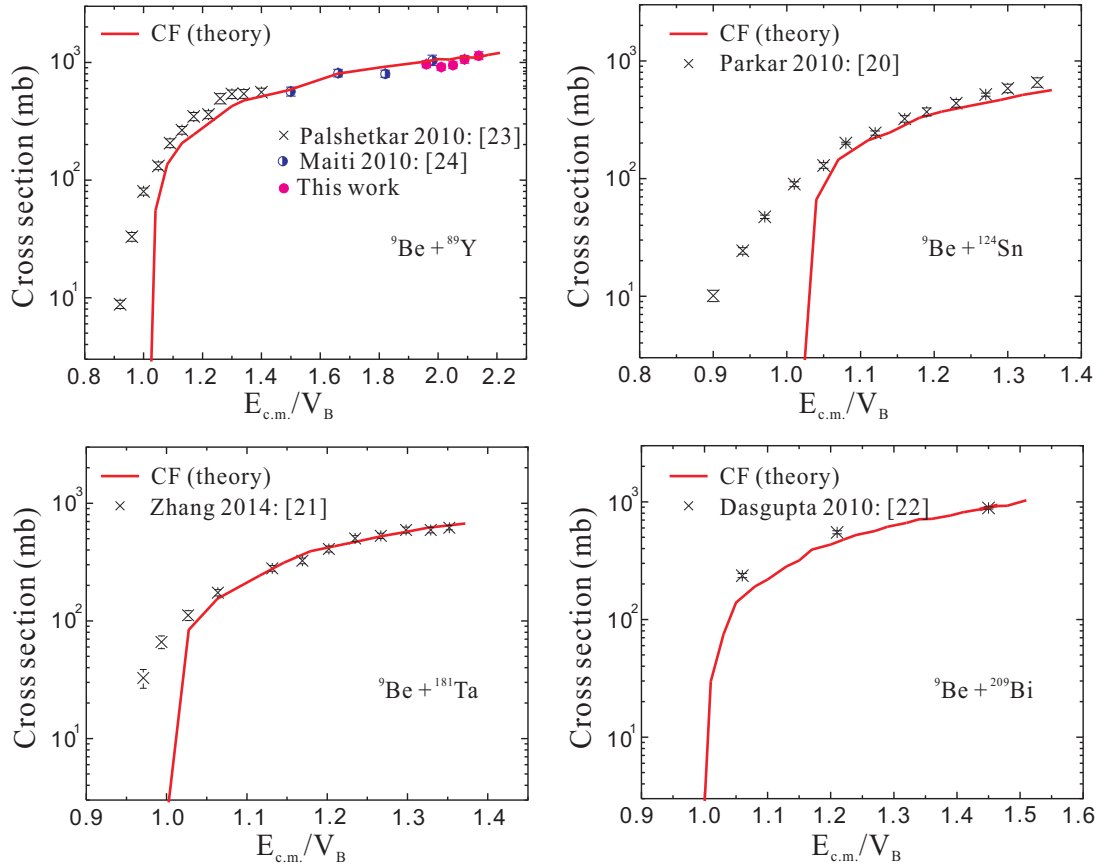


FIG. 5. Comparison of the experimental CF cross sections with the PLATYPUS predictions, for the reactions induced by ${}^9\text{Be}$ on the ${}^{89}\text{Y}$ (Refs. [23,24], and this work), ${}^{124}\text{Sn}$ [20], ${}^{181}\text{Ta}$ [21], and ${}^{209}\text{Bi}$ [22] targets. Model calculations are inadequate for energies close to the Coulomb barrier, as the quantum tunneling was not included. See text for details.

there is even one order of magnitude of discrepancy at its low-energy region for both of the level density parameters. The cause of the deviation is not understood. The reasons may come from the PACE predictions and/or previous measurement [24], but that is just the speculation. The experimental CF cross sections were deduced by dividing the cumulative measured ($\sigma_{2n+3n+4n+5n}^{\text{expt}}$) cross sections by the ratio R , which gives the missing ER contribution, if any. Here the ratio R refers to $\sum_x \sigma_{xn}^{\text{PACE}} / \sigma_{\text{fus}}^{\text{PACE}}$, where $x = 2, 3, 4, 5$, calculated with $a = A/9.6 \text{ MeV}^{-1}$ for direct comparison of extended data with the previous research [23]. The values of ratio R and the deduced CF cross sections are listed in Table III. Note that the PACE calculations gives little difference of the deduced CF cross sections with small difference of the density parameters. For example, if the parameter of $K = 13$ was adopted in the calculation, the deduced CF cross sections could be 8% higher at most in our extended energy region. For the $\alpha 2n$ and $\alpha 4n$ residues, it is not possible in our work to distinguish them between the CF and ICF processes unambiguously. In addition, the $\alpha 3n$ channel is missing, as it decays directly to the ground state of the stable daughter nucleus. Therefore, we could not deduce the total ICF cross sections, and the present work focuses on the study of CF cross sections.

The PLATYPUS code [25] that is based on a classical dynamical model is employed, to test the systematical feature of

the prompt-breakup probabilities [9,10,12] with the extended ${}^9\text{Be} + {}^{89}\text{Y}$ CF cross-section data. The model uses classical trajectories in conjunction with stochastic breakup. This is done by including a breakup function that undergoes Monte Carlo sampling. A key feature is that the integral of breakup probability along a given classical orbit is an exponential function of its distance of closest approach R_{\min} [34]:

$$P_{\text{BU}}(R_{\min}) = 2 \int_{R_{\min}}^{\infty} P_{\text{BU}}^L(R) dR = A \exp(-\alpha R_{\min}), \quad (1)$$

where $P_{\text{BU}}^L(R) dR$ is the probability of breakup in the interval R to $R + dR$, and A and α are parameters related to the reaction system. The factor of two highlights that breakup may occur along the entrance or exit branch of the trajectory. This breakup function encodes the effect of Coulomb and nuclear interactions that cause the breakup, making this approach a quantitative dynamical model for relating the sub-barrier noncapture breakup to the above-barrier ICF and CF of weakly bound nuclei, rather than a breakup model. A detailed description of the model has been presented in Refs. [34–36].

For the reaction induced by weakly bound projectiles, Bing Wang *et al.* [9] has reframed the prompt-breakup probability as:

$$P_{\text{BU}} = \exp[a + \mu(R_{\min} - R_p - R_T)], \quad (2)$$

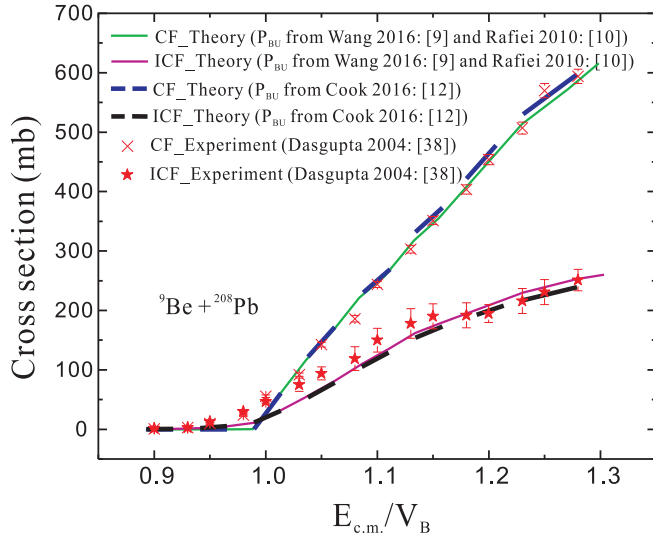


FIG. 6. Comparison of predictions of CF and ICF cross sections by the PLATYPUS model for the ${}^9\text{Be} + {}^{208}\text{Pb}$ system, using two sets of breakup probability parameters from Refs. [9,10] and Ref. [12], respectively. The experimental data, taken from Ref. [38], is also presented. See text for details.

where R_P and R_T are the radii of the equivalent spherical nuclei and can be calculated using $R_{P(T)} = r_0 A_{P(T)}^{1/3}$ with $r_0 = 1.2$ fm. They have also extracted the parameters of $\mu = -0.884$ fm $^{-1}$ and $a = 0.557$ for the ${}^9\text{Be}$ projectile from systematically fitting of the measured prompt-breakup probabilities [10], and pointed out that the effect of breakup on complete fusion is a threshold effect. Using the extracted parameters we have performed PLATYPUS calculations for the ${}^9\text{Be}$ interaction with ${}^{89}\text{Y}$, ${}^{124}\text{Sn}$, ${}^{181}\text{Ta}$, and ${}^{209}\text{Bi}$, respectively. The ${}^{124}\text{Sn}$, ${}^{181}\text{Ta}$, and ${}^{209}\text{Bi}$ targets were chosen simply because they hold different mass number compared to ${}^{89}\text{Y}$. In the calculation, the nuclear interactions between the projectile/fragments and targets were considered to be a Woods-Saxon potential, and determined from the global Broglia-Winther parametrization [37]. Figure 5 shows the calculated fusion excitation functions for the CF of four systems, as a function of $E_{c.m.}/V_B$, comparing with the corresponding experimental data. Here, $E_{c.m.}$ and V_B refer to beam energy in the center-of-mass frame and Coulomb barrier energy, respectively. The experimental cross-section data of ${}^9\text{Be}$ with ${}^{124}\text{Sn}$, ${}^{181}\text{Ta}$, and ${}^{209}\text{Bi}$ systems were taken from Refs. [20–22]. One can see from Fig. 5 the good agreements that have been achieved for the four system with different targets at above-barrier energies. The present classical dynamical model does not treat quantum tunneling, so the descriptions of the experimental data at energies close to the Coulomb barrier are not reliable.

For the ${}^9\text{Be}$ breakup function another dedicated measurement was performed, and a fairly weak Z_T dependence is reported [12]. We calculated the CF and ICF cross sections of the ${}^9\text{Be} + {}^{208}\text{Pb}$ system using the updated parameters and compared with the predictions using the previous parameters deduced by fitting the experimental data [9,10]. The comparison is shown in Fig. 6, where the experimental data [38] is

also presented. As can be seen, for the predictions there is no substantial difference between the two sets of the parameters. Note that the ${}^9\text{Be} + {}^{208}\text{Pb}$ system is the available data that holds largest difference between the two sets of parameters. Thus, from the analysis using PLATYPUS model, we conclude that in the reactions involving weakly bound ${}^9\text{Be}$ projectile the suppression of CF at above-barrier energies, including the present data of ${}^9\text{Be} + {}^{89}\text{Y}$ system up to $2 V_B$, is roughly independent of the target atomic mass. The comparison in Fig. 6 also indicates that the dedicated investigation is still needed to get the new parameterized breakup functions, and find a method to check the precision.

It should be pointed out that there are some dedicated efforts and improvements in the PLATYPUS model (e.g., by taking into account lifetimes associated with unbound states) for the study of ${}^{6,7}\text{Li}$ -induced reactions. Also, studies have revealed the importance of transfer-triggered breakup [16–18] and cluster transfer [19]. However, studies have also shown that prompt breakup of ${}^9\text{Be}$ occurs dominantly through an excited ${}^8\text{Be}$ nucleus [10]. In our calculation, ${}^8\text{Be}$ was used as a pseudoprojectile, and there are no other competing reactions such as transfer-triggered breakup process. In this work, the employed PLATYPUS model, which is based on a breakup-fusion picture, has proved to be suitable to predict the CF and ICF cross sections of ${}^9\text{Be}$ -induced reactions at above-barrier energies.

IV. SUMMARY

The excitation functions of complete fusion (CF) cross sections for the ${}^9\text{Be} + {}^{89}\text{Y}$ system have been measured at well above the Coulomb barrier energies, in the range from 45.9–50.1 MeV by employing the stacked foil activation technique and off-line γ -ray spectrometry. The extended CF data was analyzed using the PLATYPUS code that is based on a classical dynamical model, and compared with other targets of different mass involving the same projectile. It is shown that until the greater-than-barrier energies the ${}^9\text{Be} + {}^{89}\text{Y}$ system is consistent with the systematic behavior that the ${}^9\text{Be}$ prompt-breakup probability is roughly irrespective of target atomic mass, based on a breakup-capture picture within the PLATYPUS model. This study extends the information on the reactions induced by the weakly bound nuclei, and also indicates that a new parameterized ${}^9\text{Be}$ breakup function for above-barrier CF and ICF excitation functions is still required to accurately describe the reaction mechanisms.

ACKNOWLEDGMENTS

The work at Institute of Modern Physics, CAS was supported by the National Key R&D Program of China (Contract No. 2018YFA0404402), the Youth Innovation Promotion Association of Chinese Academy of Sciences (Grant No. 2019407), the Fundamental Research Funds of Chinese Academy of Sciences (Grant No. QYZDJ-SSW-SLH041), and the National Natural Science Foundation of China (Grants No. U1932138, No. 11305221, No. 11775274, and No. 11575255). The work at University of Surrey was supported by the STFC (Grant No. ST/P005314/1).

- [1] L. F. Canto, P. R. S. Gomes, R. Donangelo, J. Lubian, and M. Hussein, *Phys. Rep.* **596**, 1 (2015).
- [2] L. F. Canto, P. R. S. Gomes, R. Donangelo, and M. Hussein, *Phys. Rep.* **424**, 1 (2006).
- [3] J. Kolata, V. Guimaraes, and E. Aguilera, *Europhys. J. A* **52**, 123 (2016).
- [4] M. Dasgupta, D. J. Hinde, R. D. Butt, R. M. Anjos, A. C. Berriman, N. Carlin, P. R. S. Gomes, C. R. Morton, J. O. Newton, A. Szanto de Toledo *et al.*, *Phys. Rev. Lett.* **82**, 1395 (1999).
- [5] S. B. Moraes, P. R. S. Gomes, J. Lubian, J. J. S. Alves, R. M. Anjos, M. M. Sant'Anna, I. Padrón, C. Muri, R. Liguori Neto, and N. Added, *Phys. Rev. C* **61**, 064608 (2000).
- [6] P. R. S. Gomes, M. D. Rodríguez, G. V. Martí, I. Padron, L. C. Chamon, J. O. Fernández Niello, O. A. Capurro, A. J. Pacheco, J. E. Testoni, A. Arazi *et al.*, *Phys. Rev. C* **71**, 034608 (2005).
- [7] P. R. S. Gomes, I. Padron, M. Rodríguez, G. Martí, R. Anjos, J. Lubian, R. Veiga, R. L. Neto, E. Crema, N. Added *et al.*, *Phys. Lett. B* **601**, 20 (2004).
- [8] M. Dasgupta, D. J. Hinde, K. Hagino, S. B. Moraes, P. R. S. Gomes, R. M. Anjos, R. D. Butt, A. C. Berriman, N. Carlin, C. R. Morton *et al.*, *Phys. Rev. C* **66**, 041602(R) (2002).
- [9] B. Wang, W.-J. Zhao, A. Diaz-Torres, E.-G. Zhao, S.-G. Zhou *et al.*, *Phys. Rev. C* **93**, 014615 (2016).
- [10] R. Rafiei, R. du Rietz, D. H. Luong, D. J. Hinde, M. Dasgupta, M. Evers, and A. Diaz-Torres, *Phys. Rev. C* **81**, 024601 (2010).
- [11] S. Kalkal, E. C. Simpson, D. H. Luong, K. J. Cook, M. Dasgupta, D. J. Hinde, I. P. Carter, D. Y. Jeung, G. Mohanto, C. S. Palshetkar *et al.*, *Phys. Rev. C* **93**, 044605 (2016).
- [12] K. J. Cook, E. C. Simpson, D. H. Luong, S. Kalkal, M. Dasgupta, and D. J. Hinde, *Phys. Rev. C* **93**, 064604 (2016).
- [13] L. R. Gasques, D. J. Hinde, M. Dasgupta, A. Mukherjee, and R. G. Thomas, *Phys. Rev. C* **79**, 034605 (2009).
- [14] P. R. S. Gomes, R. Linares, J. Lubian, C. C. Lopes, E. N. Cardozo, B. H. F. Pereira, and I. Padron, *Phys. Rev. C* **84**, 014615 (2011).
- [15] V. Jha, V. V. Parkar, and S. Kailas, *Phys. Rev. C* **89**, 034605 (2014).
- [16] A. Shrivastava, A. Navin, N. Keeley, K. Mahata, K. Ramachandran, V. Nanal, V. Parkar, A. Chatterjee, and S. Kailas, *Phys. Lett. B* **633**, 463 (2006).
- [17] D. Luong, M. Dasgupta, D. Hinde, R. du Rietz, R. Rafiei, C. Lin, M. Evers, and A. Diaz-Torres, *Phys. Lett. B* **695**, 105 (2011).
- [18] D. H. Luong, M. Dasgupta, D. J. Hinde, R. du Rietz, R. Rafiei, C. J. Lin, M. Evers, and A. Diaz-Torres, *Phys. Rev. C* **88**, 034609 (2013).
- [19] K. J. Cook, E. C. Simpson, L. T. Bezzina, M. Dasgupta, D. J. Hinde, K. Banerjee, A. C. Berriman, and C. Sengupta, *Phys. Rev. Lett.* **122**, 102501 (2019).
- [20] V. V. Parkar, R. Palit, S. K. Sharma, B. S. Naidu, S. Santra, P. K. Joshi, P. K. Rath, K. Mahata, K. Ramachandran, T. Trivedi *et al.*, *Phys. Rev. C* **82**, 054601 (2010).
- [21] N. T. Zhang, Y. D. Fang, P. R. S. Gomes, J. Lubian, M. L. Liu, X. H. Zhou, G. S. Li, J. G. Wang, S. Guo, Y. H. Qiang *et al.*, *Phys. Rev. C* **90**, 024621 (2014).
- [22] M. Dasgupta, D. J. Hinde, S. L. Sheehy, and B. Bouriquet, *Phys. Rev. C* **81**, 024608 (2010).
- [23] C. S. Palshetkar, S. Santra, A. Chatterjee, K. Ramachandran, S. Thakur, S. K. Pandit, K. Mahata, A. Shrivastava, V. V. Parkar, and V. Nanal, *Phys. Rev. C* **82**, 044608 (2010).
- [24] M. Maiti and S. Lahiri, *Phys. Rev. C* **81**, 024603 (2010).
- [25] A. Diaz-Torres, *Comput. Phys. Commun.* **182**, 1100 (2011).
- [26] Y. D. Fang, P. R. S. Gomes, J. Lubian, M. L. Liu, X. H. Zhou, D. R. Mendes Jr., N. T. Zhang, Y. H. Zhang, G. S. Li, J. G. Wang *et al.*, *Phys. Rev. C* **91**, 014608 (2015).
- [27] D. Bazin, O. Tarasov, M. Lewitowicz, and O. Sorlin, *Nucl. Instr. Meth. Phys. Res. A* **482**, 307 (2002).
- [28] C. Scheidenberger and H. Geissel, *Nucl. Instr. Meth. Phys. Res. B* **135**, 25 (1998).
- [29] G. S. Li, Y. D. Fang, A. Diaz-Torres, M. L. Liu, N. T. Zhang, X. H. Zhou, Y. H. Zhang, J. G. Wang, B. S. Gao, Y. H. Qiang *et al.*, *Phys. Rev. C* **99**, 054617 (2019).
- [30] ENSDF-NNDC-BNL (US), URL <http://www.nndc.bnl.gov/ensdf/>.
- [31] R. A. Meyer, K. V. Marsh, D. S. Brenner, and V. Paar, *Phys. Rev. C* **16**, 417 (1977).
- [32] A. Gavron, *Phys. Rev. C* **21**, 230 (1980).
- [33] K. Hagino, N. Rowley, and A. Kruppa, *Comput. Phys. Commun.* **123**, 143 (1999).
- [34] A. Diaz-Torres, *J. Phys. G: Nucl. Part. Phys.* **37**, 075109 (2010).
- [35] A. Diaz-Torres, D. J. Hinde, J. A. Tostevin, M. Dasgupta, and L. R. Gasques, *Phys. Rev. Lett.* **98**, 152701 (2007).
- [36] A. Diaz-Torres and D. Quraishi, *Phys. Rev. C* **97**, 024611 (2018).
- [37] W. Reisdorf, *J. Phys. G: Nucl. Part. Phys.* **20**, 1297 (1994).
- [38] M. Dasgupta, P. R. S. Gomes, D. J. Hinde, S. B. Moraes, R. M. Anjos, A. C. Berriman, R. D. Butt, N. Carlin, J. Lubian, C. R. Morton *et al.*, *Phys. Rev. C* **70**, 024606 (2004).